Chapter 6

Application of PANI-PVA nanofiber based electrodes for electrochemical biosensing of Glucose and Aflatoxin B_1

This chapter emphasizes the development of electrochemical sensors utilizing PANI-PVA nanofibers for detecting glucose and AF-B_1 with high specificity and versatility. The electrochemical characterization of the sensor electrodes was performed using Cyclic Voltammetry (CV) and Electrochemical Impedance Spectroscopy (EIS), while chronoamperometry was employed for the amperometric detection of glucose. For AF-B_1 detection, both capacitive and amperometric techniques were utilized to evaluate the key sensing parameters. Critical biosensor performance metrics, including sensitivity, selectivity, limit of detection, linearity and reliability, were thoroughly assessed for both sensor types. The practical applicability of the developed biosensors was validated through real sample analysis, demonstrating their potential for real-world applications.

6.1. Introduction

The introduction of nanotechnology into sensor development has led to remarkable improvements that are unattainable with traditional microfabrication methods [1]. Nanostructures such as nanotubes, nanowires, nanofibers, quantum dots, and nanoparticles can be integrated into biosensor components, enhancing their performance significantly. Among these, nanofibers have become increasingly popular in analytical systems as sensing elements [2,3]. Their high surface area, flexibility, porosity, and good mechanical properties make them efficient for improving biosensor functionality [4,5]. Nanofibers offer abundant immobilization sites for biomolecules, enhancing interactions and significantly lowering detection limits. Additionally, their high porosity facilitates rapid biomolecule penetration, effectively reducing detection time [6]. These properties allow for the development of nanofibrous sensing films that exhibit exceptional sensitivity and selectivity towards various analytes [7]. Additionally, the nanofibrous structure is ideal for incorporating high concentrations of enzymes, which significantly enhances biosensing performance [8-9].

Polyaniline (PANI) was the first commercially available conducting polymer and has since been extensively studied for a wide range of applications, including batteries, chemical sensors, and biosensors [10]. Its widespread use in biosensor design is attributed to its distinctive properties, particularly its capability to enhance electron transfer during redox or enzymatic reactions. Additionally, PANI serves as an excellent matrix for biomolecular immobilization [11,12]. Its prominence in the field of biosensors is also

attributed to its high conductivity, redox reversibility, long-term environmental stability, solution processability, and simple synthetic methods that allow precise control of its thickness on sensor electrodes [13]. PANI can be synthesized into various nanostructures—such as nanospheres, nanofibers, nanowires, nanorods, and nanotubes [14,15]. Among all, PANI nanofibers have garnered significant attention for potential commercial uses in areas such as batteries, sensors, molecular electronics, separation membranes, corrosion inhibitors, electrochromic devices, energy storage systems, field emission, and digital memory devices due to its tremendous properties [16,17]. Several methods have been developed for fabricating 1D nanostructures, with electrospinning being a versatile, cost-effective technique capable of producing nanofibers with a large specific surface area [18]. This extensive surface area offers the potential for ultra-high sensitivity and rapid response times in sensing applications. Although PANI is an excellent conducting polymer, its processability into fiber mats through electrospinning is challenging due to its limited solubility in common solvents. To address these issues, extensive efforts have been made to blend PANI with more soluble polymers such as polyvinyl alcohol (PVA), poly (styrene sulfonate) (PSS), polymethyl methacrylate (PMMA), and polyethylene oxide (PEO) [19-21]. In this study, blending PANI with PVA effectively overcomes these challenges. PVA not only provides good film-forming ability but also ensures a homogeneous dispersion by forming hydrogen bonds with PANI [22]. Additionally, PVA is a semicrystalline polyhydroxy polymer that has been widely studied and used as a binding material in electrospinning due to its water solubility, biocompatibility, thermal stability, biodegradability, and excellent physical properties [23,24].

In this chapter, PANI-PVA nanofibers have been employed as an electrode material to further enhance the sensing parameters, especially, the dynamic concentration range of the biosensors. The sensing activity of the glucose sensor was evaluated using chronoamperometry technique. Additionally, both amperometric and capacitive measurements are explored for the detection of AF-B_1.

(A) Glucose sensor

6.2. Electrochemical studies of the glucose biosensors

To investigate the interfacial charge transfer kinetics at each step of the sensor fabrication process, EIS and CV were performed. The CV was conducted on the prepared PANI-PVA/ITO at a scan rate of 20 mV/s within a potential window of -0.4 V to 1.0 V [25], using 0.1 M phosphate buffer saline (PBS) as the electrolyte (pH-7.4). Additionally, multifrequency impedance spectroscopy was performed on the composite electrodes after each fabrication step, employing an AC signal of 10 mV across a frequency range of 1 Hz to 1 MHz in the PBS electrolyte (pH=7.4). The interaction between glucose and glucose oxidase was observed through amperometric measurements using chronoamperometry.

6.2.1. Cyclic voltammetry (CV) studies of glucose sensor

The CV curves for the PANI-PVA/ITO electrode following each step of the sensor fabrication process, including glutaraldehyde treatment, enzyme (glucose oxidase) immobilization, and enzyme-glucose interaction, are presented in Figure 6.1. After glutaraldehyde treatment, a noticeable decrease in the area under the CV curve is observed, indicating reduced charge transfer at the interface. This reduction is attributed to the formation of a thin glutaraldehyde layer, which hinders electron movement across the electrode surface. Similarly, the immobilization of glucose oxidase further limits charge transfers due to the large molecular size of the enzyme. The bulky structure of the enzyme creates a barrier at the interface, leading to a significant decrease in the area under the CV curve. This step highlights how the enzyme layer impacts the electrochemical properties of the electrode by introducing resistance to charge transport. However, upon the interaction between glucose oxidase and the analyte glucose, the CV plot undergoes a transformation. A new oxidation peak emerges around 0.5 V, signifying a catalytic reaction between the enzyme and glucose [26]. This peak is indicative of the oxidation of glucose, facilitated by glucose oxidase, which enhances the charge transfer process. The appearance of this peak demonstrates the sensor's ability to detect glucose and reflects the improved electrochemical activity due to the enzymatic reaction.

The changes observed in the CV curves are attributed to the interaction between glucose and the co-enzyme flavin adenine dinucleotide (FAD) within glucose oxidase (*GlOx*) [27-29]. The FAD participates in a redox reaction with biomolecules, involving the transfer of two electrons and two protons, as outlined in Equation 4.1, Chapter 4.

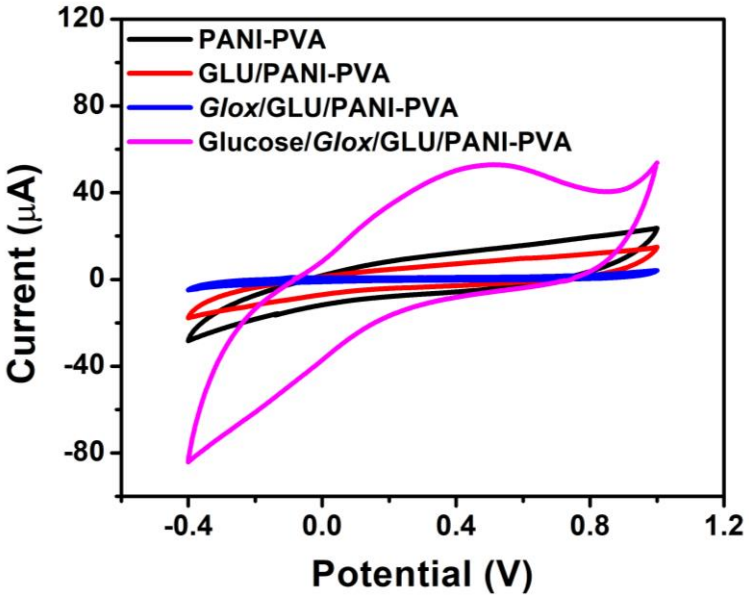

Figure 6.1: Cyclic voltammetry plots of *GlOx*/GLU/PANI-PVA/ITO sensor after each process step, with final step of 460.87 μM glucose interaction.

GlOx catalyzes the conversion of glucose into D-glucono-1,5-lactone by transferring two protons and two electrons from glucose to FAD, leading to the formation of $FADH_2$. When glucose is introduced, the enzyme-catalyzed reaction between FAD and glucose results in an increased oxidation peak current, as demonstrated by the following equation

$$\text{Glucose} + \textit{GlOx}\ (\text{FAD}) \rightarrow \text{Gluconolactone} + \textit{GlOx}\ (\text{FADH}_2) \qquad (6.1)$$

The increase in oxidation peak is attributed to oxidation of H_2O_2, which is released as a result of enzymatic reaction of glucose oxidase with glucose, details explained in chapter 5.

6.2.2. Electrochemical impedance studies of glucose sensor

The impedance spectra for the PANI-PVA/ITO electrodes are presented in Figure 6.2, illustrating the changes after each sensor fabrication step, including glutaraldehyde treatment, enzyme immobilization, and the enzyme-glucose interaction. The equivalent circuit parameters are defined as follows: R_1 represents the series resistance, which includes solution resistance, while R_{ct} denotes the charge transfer resistance. The capacitor C_2 corresponds to the formation of a double-layer capacitor at the interface. Additionally, W_3 indicates the Warburg impedance, which arises from diffusion within the polymer structure. The values of the equivalent circuit parameters are tabulated in Table 6.1.

Table 6.1: Fitted parameters from EIS spectra for PANI-PVA/ITO electrode after every process step of sensor fabrication.

Serial number	Electrode	R_1 (Ω)	R_{ct} (Ω)	$C_2(\times10^{-6})$ $S.s^n$	$W_3(x10^{-6})$ $(S.s^{1/2})$
1	PANI-PVA	36.31	99.58	3.589	1380
2	GLU/PANI-PVA	50.17	440.3	4.391	1551
3	*Glox*/GLU/PANI-PVA	43.35	1189	7.157	2951
4	Glucose/*Glox*/GLU/PANI-PVA	47.04	588.5	6.781	1405

The R_{ct} value for the PANI-PVA electrode increased from 99.58 Ω to 440.3 Ω following glutaraldehyde treatment. After the immobilization of the *GlOx* enzyme, the R_{ct} value further raised to 1189 Ω, attributed to the adsorption of the enzyme on the surface of the GLU/PANI-PVA. However, after the interaction between the enzyme and glucose, the R_{ct} value decreased to 588.5 Ω, indicating improved charge transport at the interface as glucose oxidase facilitates the oxidation of glucose.

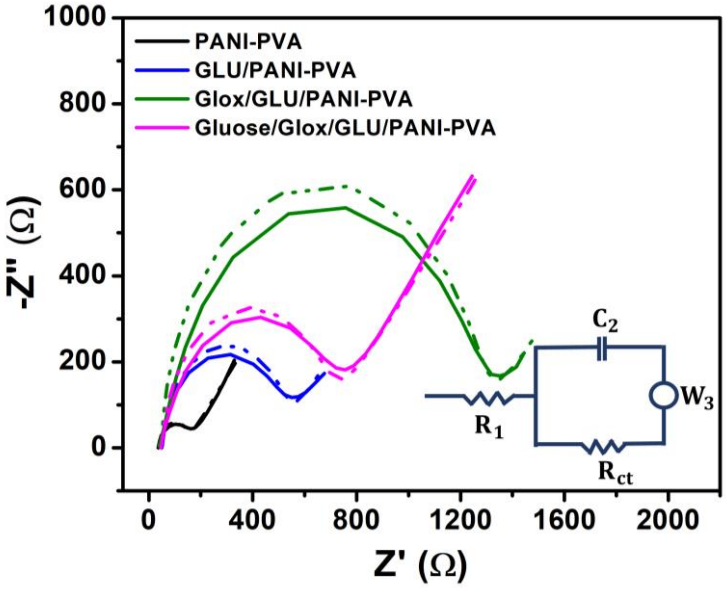

Figure 6.2: Impedance response of PANI-PVA/ITO sensor (with addition of glucose concentration 460.87 μM) after each process steps.

The Q_2 value, which reflects the capacitance of the double-layer capacitor, steadily increases following the glutaraldehyde treatment and the deposition of the enzyme layer. However, when the enzyme interacts with glucose, a slight decrease in the Q_2 value occurs, suggesting an improvement in charge transfer efficiency. This reduction indicates that the enzymatic reaction facilitates a more effective movement of charge at the interface, thereby enhancing the overall electrochemical response. The W_3 value increases after glutaraldehyde treatment and subsequent enzyme immobilization occurs due to an increase in diffusional impedance. This rise is indicative of the enhanced resistance to the diffusion of ions through the modified electrode surface, which occurs as the glutaraldehyde creates a cross-linked network, effectively trapping the enzyme and potentially hindering the movement. However, following the interaction between the enzyme and the analyte, the W_3 value decreases. This reduction signifies an improvement in the diffusion characteristics at the electrode interface, which can be attributed to the catalytic activity of the enzyme. As glucose oxidase interacts with glucose, it facilitates the conversion of glucose to D-glucono-1,5-lactone, generating products that allow for more efficient charge transport and diffusion within the modified electrode. This dynamic interaction leads to a lower diffusional impedance, enhancing the overall electrochemical response of the sensor.

6.3. Glucose oxidation performance of the fabricated sensor electrode

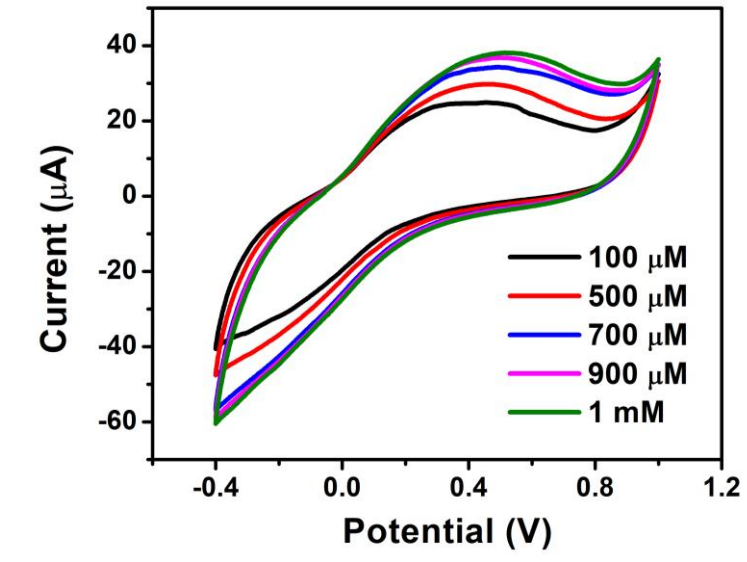

Figure 6.3: Cyclic voltammetry plot of *Glox*/GLU/PANI-PVA bioelectrode at different glucose concentrations.

CV plots were obtained using the glucose oxidase-immobilized PANI-PVA/ITO electrode at various glucose concentrations, as illustrated in Figure 6.3. The CV was conducted with various glucose concentrations of 100 µM, 500 µM, 700 µM, 900 µM, and 1 mM in a PBS electrolyte. A notable increase in the oxidation peak current is clearly observed across different glucose concentrations within the potential range of 0.4 V to 0.5 V.

6.4. Sensing of glucose via chronoamperometry

To enable rapid and direct measurement of glucose concentrations, amperometric studies were conducted on the prepared electrodes using chronoamperometry. The amperometric response for the glucose oxidase-immobilized GLU/PANI-PVA electrode is illustrated in Figure 6.4 (a), where glucose was injected at different time intervals. Chronoamperometry was carried out at a working potential of 0.5 V versus Ag/AgCl for the GLU/PANI-PVA/ITO electrode with glucose oxidase immobilized. With each incremental addition of glucose, the baseline demonstrated a corresponding rise in current response at each stage. To further evaluate the selectivity of the sensor, ascorbic acid was introduced at position A during the experiment. Despite the addition of ascorbic acid (20 µL), the sensor exhibited no significant change in current response, confirming its high selectivity for glucose over interfering substances such as ascorbic acid. The variation in current response with increasing glucose concentration for the *Glox*/GLU/PANI-PVA sensor is depicted in Figure 6.4 (b). A linear regression fit ($R^2 = 0.9920$) was applied to the data, with a 2.3% error margin (as shown in Figure 6.4 (b)). The LOD of the sensor was calculated using the formula $LOD = 3.3\times\sigma/m$, where σ represents the standard deviation and m is the slope of the regression line [30]. The LOD was determined to be 1.65 µM, with a sensitivity of 17.7 µA μM^{-1}. Additionally, the sensor demonstrated a broad linear range from 0.19 to 455.42 µM for glucose oxidation. To compare with clinical glucose estimates, the linear regression plot ($R^2 = 0.9975$) illustrating the relationship between concentration (both in µM and mg/dL) and the change in current (ΔI) for the PANI-PVA/ITO sensors is presented in Figure 6.4 (c). The PANI-PVA/ITO sensor exhibited a linear range between 0.00342 mg/dL and 8.19 mg/dL. The study demonstrated that the linear concentration range for the PANI-PVA/ITO sensor exceeds that of most reported enzymatic glucose sensors, including those detailed in our previous studies in Chapter 4 and Chapter 5. PANI nanofibers exhibit an enhanced linear range for glucose detection compared to AuNP/GO/PEDOT-PSS and AuNP/WS_2/PEDOT-PSS due to their structural advantages and stable enzyme immobilization.

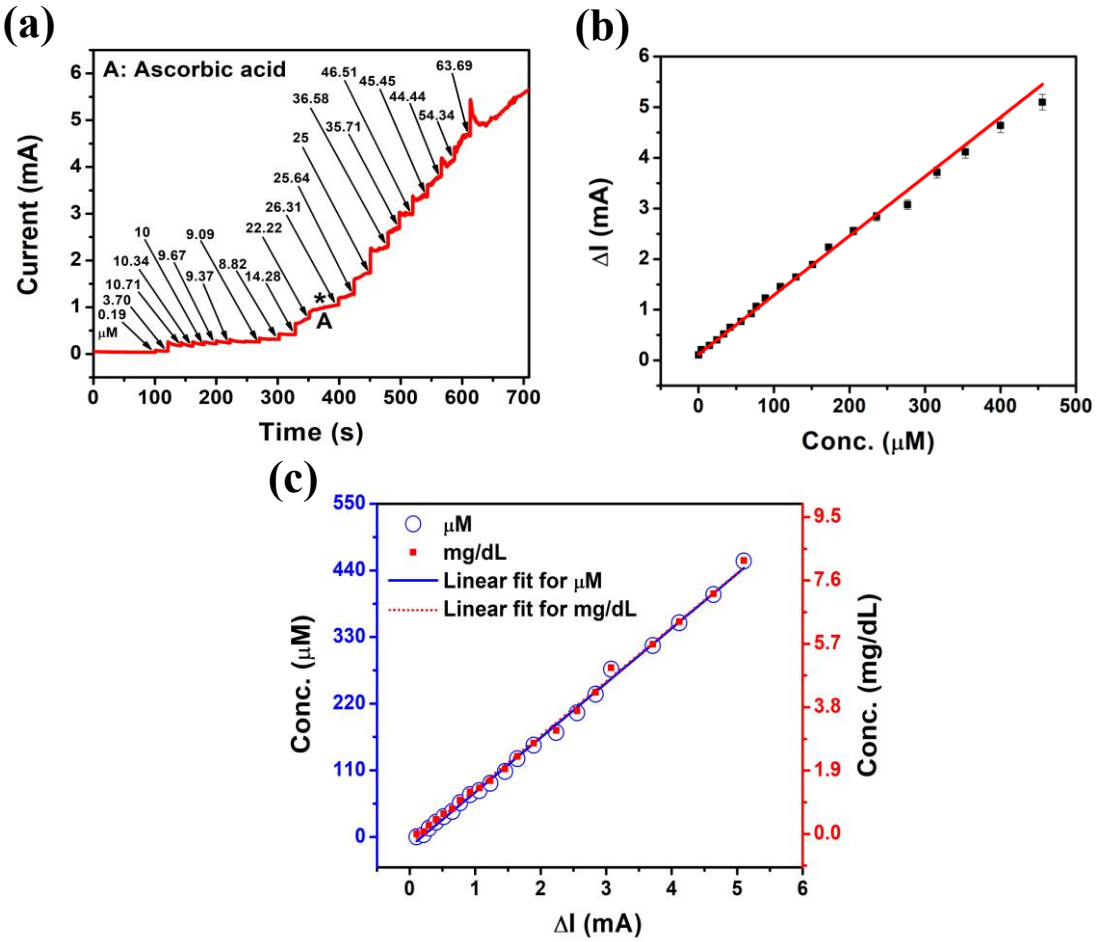

Figure 6.4: (a) Chronoamperometry plots of PANI-PVA/ITO electrode at different concentrations of glucose. (b) Linear regression plot of current vs. concentration for PANI-PVA /ITO biosensor with error bar. (c) Linear regression plot of Conc. (both μM and mg/dL) vs ΔI for PANI-PVA /ITO.

However, they experience lower sensitivity and higher LOD compared to the AuNP/WS_2/PEDOT-PSS composite, which may be due to less favourable electron transfer dynamics, limited enzyme accessibility, increased interference, and potentially reduced enzymatic activity. These factors collectively influence the electrochemical performance of the respective sensors in enzymatic glucose detection.

6.5. Selectivity and repeatability of the sensor electrode

The selectivity of the *Glox*/GLU/PANI-PVA sensor was rigorously evaluated by testing its response to various potential interfering species, such as ascorbic acid, sucrose, and uric acid, each at a concentration of 1 mM. As illustrated in Figure 6.5, the sensor demonstrated remarkable selectivity, as there was no significant change in the baseline current upon the

introduction of these interfering compounds. This indicates that the sensor can effectively differentiate glucose from other common substances that may be present in biological samples, ensuring accurate glucose measurements. To further validate the reliability of the sensor, repeatability studies were conducted using three different PANI-PVA/ITO electrodes. The results of these experiments, displayed in Table 6.2, provide insight into the consistency of the sensor's performance across multiple repetitions.

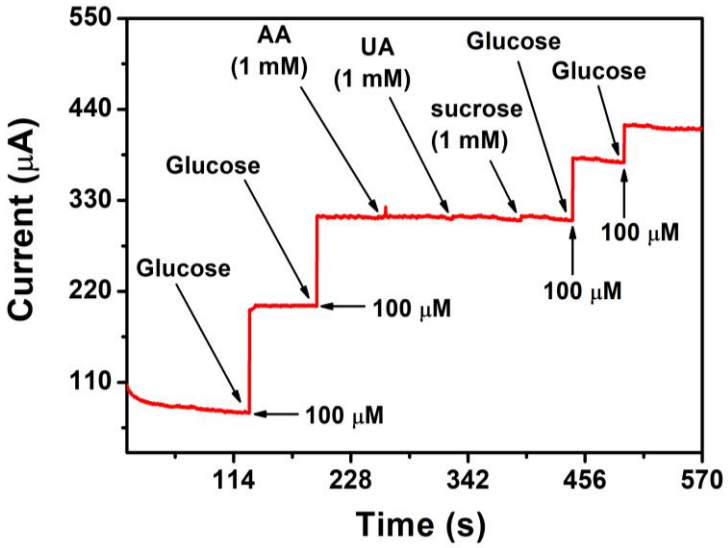

Figure 6.5: Selectivity test of PANI-PVA sensor in presence of different interference like ascorbic acid (AA), uric acid (UA), sucrose (1 mM of each).

Table 6.2: Results of PANI-PVA glucose sensor from repeatable experiment.

Serial number	Electrode	LOD (μM)	Sensitivity (μA μM^{-1})	Linear range (μM)
1	PANI-PVA, sensor 1	1.65	11.7	0.19-455.42
2	PANI-PVA, sensor 2	2.56	10.45	0.19-430.54
3	PANI-PVA, sensor 3	1.9	11.23	0.19-440.15

6.6. Real sample test

To demonstrate the potential biomedical applications of *Glox*/GLU/PANI-PVA/ITO biosensor, glucose levels in human saliva were assessed. The study involved two volunteers: one non-diabetic (Sample 1) and one diabetic (Sample 2). Both saliva samples were collected in the morning, prior to any food intake, to ensure accurate measurement of glucose content, details being described in chapter 4. Chronoamperometry was employed to assess glucose levels in the prepared saliva samples using the *Glox*/GLU/PANI-PVA/ITO electrodes. The technique involved, systematically injection of varying volumes of the saliva solution at designated time intervals after establishing a stable baseline current. This method allowed for real-time monitoring of the electrochemical response corresponding to glucose concentrations in the saliva. The chronoamperometry plots for both Sample 1 (non-diabetic) and Sample 2 (diabetic) are depicted in Figure 6.6 (a) and (b), respectively. These plots illustrate the current response over time as the saliva samples were added, providing insights into the ability of the sensor to detect glucose in real biological fluids.

The results were further analyzed through linear regression to establish a correlation between the change in current and the glucose concentration (both µM and mg/dL) in both samples (R^2: 0.9924 & 0.9836). The corresponding linear regression plots are shown in Figure 6.6 (e) and (f) for Sample 1 and Sample 2, respectively.

From the analysis, Sample 1 revealed a maximum glucose concentration of 47.56 µM (equivalent to 0.856 mg/dL), indicating a normal glucose level consistent with non-diabetic individuals. In contrast, Sample 2 exhibited a significantly higher glucose concentration of 173.42 µM (3.121 mg/dL), which aligns with expected levels in diabetic individuals.

To validate the performance of the sensor, repeatability studies were conducted. These experiments confirmed the reliability of the glucose measurements, and the results were presented with error bars in the linear regression plots (Figure 6.6 (b) and (c)). The minimal variation in readings reinforces the robustness of the *Glox*/GLU/PANI-PVA/ITO biosensor, making it a promising tool for real-time glucose monitoring in diverse biological samples.

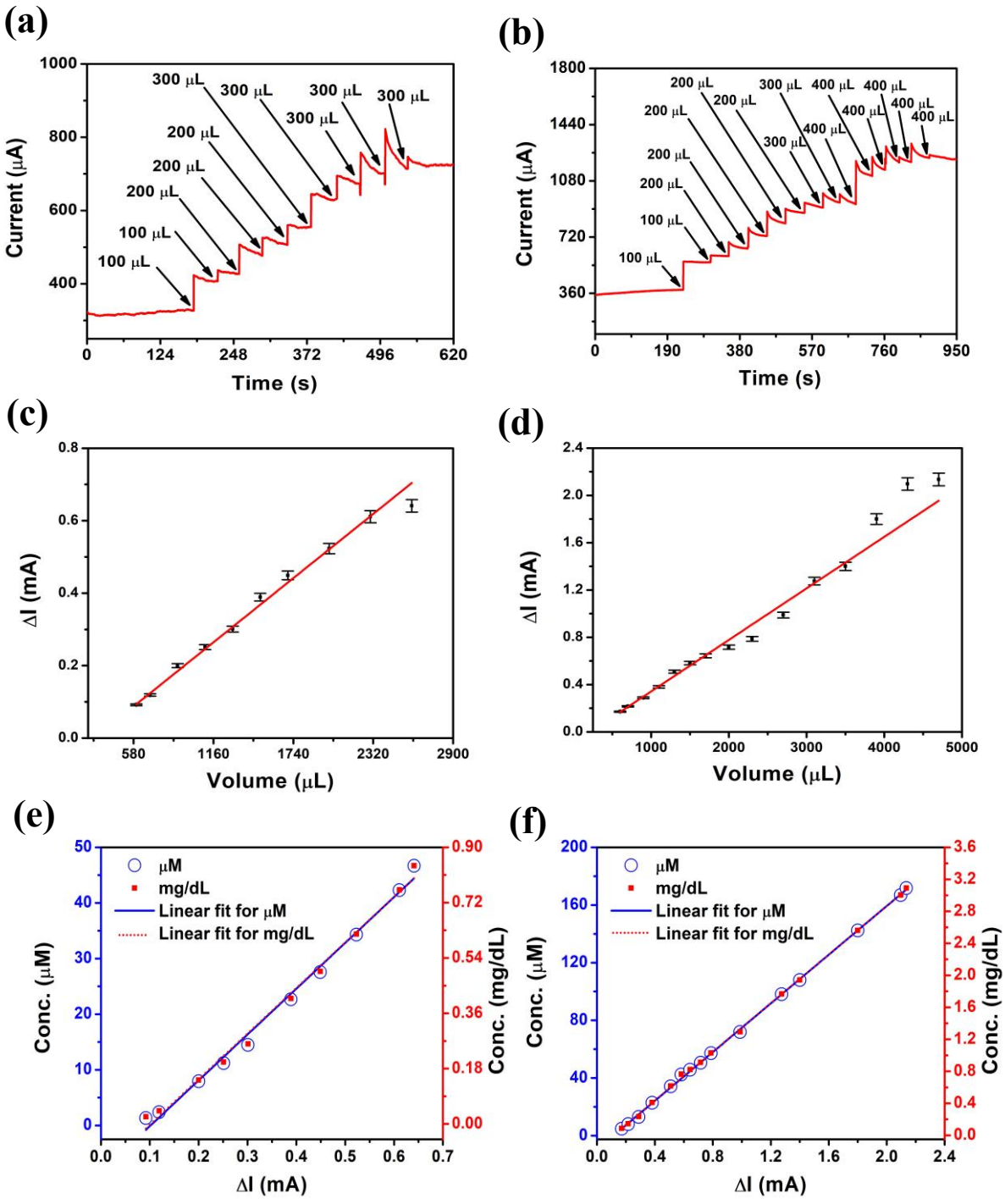

Figure 6.6: Chronoamperometry plots of PANI-PVA/ITO electrode at different volume of salivary sample (a) sample 1, (b) sample 2. Linear regression plot of current vs. volume for PANI-PVA/ITO electrode of (c) sample 1, (d) sample 2 with error bars. Linear regression plot of Conc. (both μM and mg/dL) vs ΔI (e) sample 1 and (f) sample 2.

(B) Aflatoxin B_1 sensor

6.7. Electrochemical studies of the AF-B_1 immunosensors

CV measurements were taken at each stage of sensor fabrication for the PANI-PVA electrode, using 0.1 M PBS as the electrolyte. The experiments were conducted at a scan rate of 20 mV/s, with a potential window ranging from -0.4 to 1.0 V [25]. Additionally, EIS was performed over a frequency range of 1 Hz to 1 MHz, using a 10 mV AC signal and a 0 V DC bias. The detection of AF-B_1 antigen was carried out using two techniques: transient capacitance measurements at 77 Hz and 1 kHz, along with differential pulse voltammetry (DPV).

6.7.1. Cyclic voltammetry studies of Aflatoxin B_1 sensor

The electrochemical properties of the PANI-PVA/ITO electrodes were evaluated at each stage of the sensor fabrication process, including glutaraldehyde attachment, antibody immobilization, and antigen binding, using CV. These measurements were conducted within a potential range of -0.4 V to 1.0 V, at a scan rate of 20 mV/s. The CV spectrum for the PANI-PVA/ITO electrode is presented in Figure 6.7 (a). As observed, the CV curve shows a reduction in the area after the glutaraldehyde layer was adsorbed onto the surface of the PANI-PVA/ITO electrode. This reduction is attributed to a decrease in charge transfer at the electrode interface, as the glutaraldehyde layer acts as a barrier that limits electron flow. Following this, the CV response further decreased after the immobilization of antibodies and subsequent antibody-antigen interaction. This is due to the formation of a dielectric layer at the interface, which impedes electron transfer between the electrode and the electrolyte. The dielectric layer, formed by the immobilized antibodies and antigen binding, reduces the conductivity, making it more difficult for electrons to move freely across the electrolyte-electrode interface. The formation of this insulating layer is crucial as it confirms the binding of biomolecules, which is a key aspect of the biosensor's function.

In addition to this, CV measurements were performed using the PANI-PVA/ITO electrode within a potential window from -0.4 V to 0.8 V in the presence of an another electrolyte composed of PBS and the redox couple $[Fe(CN)_6]^{3-/4-}$, as shown in Figure 6.7 (b).

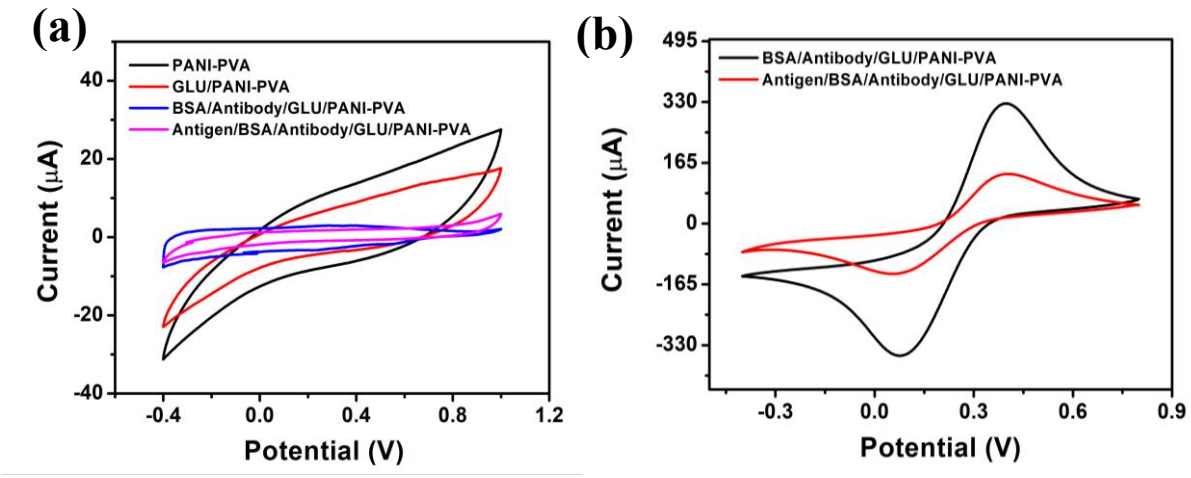

Figure 6.7: Cyclic voltammetry plot of anti-AF-B_1/PANI-PVA/ITO at a scan rate of 20 mV/s (a) within a potential window of -0.4 V to 1.0 V in PBS (electrolyte1) after each process step, with final step of injecting antigen concentration (b) within a potential window of -0.4 V to 0.8 V in 100 mM PBS and 5 mM $[Fe(CN)_6]^{3-/4-}$ (electrolyte 2) after AF-B_1 addition.

The modified electrodes demonstrated well-defined redox peaks, which are attributed to the reversible electron transfer between the electrode and the $[Fe(CN)_6]^{3-/4-}$ species in solution, corresponding to the redox reaction [Fe(III) ↔ Fe(II) + e^-] [31]. These redox peaks are indicative of efficient electron transfer at the interface. However, the area under the CV curves consistently decreases after the interaction between anti-AF-B_1 and AF-B_1, further indicating a reduction in charge transfer at the electrode surface. This decrease is associated with the formation of an immunocomplex at the surface, which further slows down electron movement at the electrode-electrolyte interface. The immunocomplex formation, resulting from the binding of the AF-B_1 antigen to the immobilized antibodies, increases the overall resistance of the system, reducing the current observed in the CV and thus confirming fruitful antigen detection.

6.7.2. Electrochemical impedance studies of Aflatoxin B_1 sensor

EIS is a powerful and effective technique for analyzing various features of electrodes, particularly after surface modifications. The impedance spectra for the PANI-PVA/ITO electrode, taken after each stage of sensor fabrication—glutaraldehyde treatment, antibody incubation, and antibody-antigen immunocomplex formation are displayed in Figure 6.8.

The Nyquist plots generated from the EIS data consist of a semicircular region and a diffusion region, representing high-frequency and low-frequency responses, respectively. The semicircular portion reflects charge transfer processes at the electrode interface, while the linear region at lower frequencies is indicative of diffusion-controlled processes. In these plots, dotted lines represent the fitted data based on an equivalent circuit model used to interpret the impedance results. This model helps in understanding the various components contributing to the overall impedance of the system. Details about the equivalent circuit parameters can be found in section 6.2.2, fitted parameters values are presented in Table 6.3. Initially, the charge transfer resistance (R_{ct}) of the unmodified PANI-PVA/ITO electrode was measured at 98.80 Ω. After treatment with glutaraldehyde, the R_{ct} value increased significantly to 362.7 Ω. This rise is attributed to the formation of a thin neutral layer of glutaraldehyde on the electrode surface, which obstructs electron flow at the interface. Glutaraldehyde, being an insulating layer, hinders charge transfer and thus increases the resistance. Following antibody immobilization, the R_{ct} value further increased to 738.8 Ω, indicating effective attachment of anti-AF-B_1 antibodies to the surface. This additional increase suggests that the antibodies form an insulating layer on the electrode, further inhibiting electron movement. After the interaction with the AF-B_1 antigen, the R_{ct} value reached 961 Ω. This substantial increase is due to the formation of a dielectric immunocomplex layer at the electrode-electrolyte interface, further obstructing electron transfer and confirming antigen binding. In addition to the charge transfer resistance, the double-layer capacitance (C_2) also showed notable changes throughout the fabrication process. After glutaraldehyde treatment, there was an observable increase in Q_2, which is likely due to the presence of reactive di-aldehyde groups on the electrode surface. These groups increase the electroactive surface area, thereby enhancing the double layer capacitance at the interface. After antibody immobilization, further increase in Q_2 was noted, confirming the effective attachment of biomolecules (antibodies) to the electrode. A significant increase in Q_2 was observed after antigen interaction, which can be attributed to the formation of the antibody-antigen complex. This complex is closely bound, and its formation likely induces conformational changes in the protein structure, further affecting the capacitance. Moreover, the Warburg impedance (W_3) values showed a consistent increase after each processing step. This rise in W_3 suggests a notable increase in diffusional resistance most likely due to the formation of porous layers during the modification process. Each modification whether the addition of glutaraldehyde,

antibodies, or the immunocomplex introduces new structures that would create barriers to diffusion. These barriers, associated with conformational changes in the antibody-antigen complex, slow down the movement of electroactive species, contributing to the overall increase in impedance.

Therefore, the impedance analysis reveals important details about the electrode modification process. The increase in R_{ct} and W_3 values after each step indicates effective surface functionalization and antigen binding, while the variations in Q_2 reflect changes in the interfacial properties due to molecular interactions. These findings provide strong evidence of the sensor's ability to detect AF-B_1 antigen based on the observed impedance changes at each processing stage.

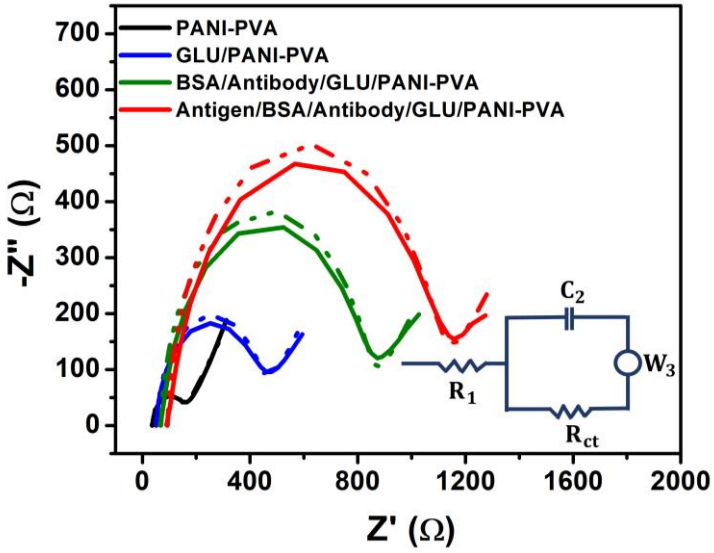

Figure 6.8: Impedance plot of PANI-PVA films on ITO electrode after each process. The inset shows the equivalent circuit.

Table 6.3: Fitted parameters of impedance spectra for PANI-PVA/ITO electrode after every process step and after addition of AF-B_1.

Serial number	Electrode	R_1 (Ω)	R_{ct} (Ω)	$C_2(\times10^{-6})$ $S.s^n$	$W_3(x10^{-6})$ $(S.s^{1/2})$
1	PANI-PVA	36.35	98.80	3.940	1490
2	GLU/PANI-PVA	51.26	362.7	4.390	1697
3	BSA/Antibody/GLU/PANI-PVA	68.21	738.8	4.987	2789
4	Antigen/BSA/Antibody/GLU/PANI-PVA	92.73	961	9.915	3132

6.8. Detection of AF-B_1 via Capacitive immunosensing and selectivity test

In a label-free immunosensor, which operates without the use of enzymes or redox agents, the detection of antigen-antibody interactions is based on measuring changes in transient capacitance. These changes arise due to the formation of an additional dielectric layer on the electrode surface as a result of antigen-antibody binding. This process creates an insulating barrier at the electrode-electrolyte interface, which can be detected by monitoring the capacitance at medium or low frequencies [25]. Since the interaction between electrodes and electrolytes leads to the formation of an electrolytic capacitor, analyte detection is carried out by measuring the transient capacitance (i.e., parallel capacitance versus time). To capture the capacitive response, measurements are performed at two different frequencies: 77 Hz, representing a lower frequency, and 1 kHz, a medium frequency. These frequencies are chosen to provide a broader analysis of the sensor's performance across varying conditions. The transient capacitance plots at both 77 Hz and 1 kHz are presented in Figure 6.9 (a) and (b), respectively. After achieving a stable baseline, the antigen AF-B_1 is progressively introduced into the PBS electrolyte, and the capacitance response is recorded. With each subsequent addition of AF-B_1, the capacitance shows a systematic decrease. This trend is attributed to the antigen-antibody binding at the interface, which leads to the formation of a dielectric layer that restricts the movement of charges at the electrode surface. As the dielectric layer thickens due to antigen binding, the capacitance decreases because the layer acts as an insulator, hindering electron flow. To assess the selectivity of the immunosensor, human serum IgG, a non-specific protein that does not interact with the anti-AF-B_1 antibody, is introduced. At 77 Hz, an initial rise in the capacitive response is observed upon the addition of IgG, but the response quickly returns to the previous trend, indicating that IgG does not form a stable bond with the sensor. At 1 kHz, no significant change in the capacitive response is detected when IgG is added, further confirming the absence of interaction with anti-AF-B_1. These results demonstrate the high specificity of the immunosensor towards the AF-B_1 antigen, as there are no notable changes in capacitance in the presence of non-specific proteins, regardless of the frequency.

Next, the change in capacitance (ΔC_p) at each step of antigen addition is plotted against antigen concentration for both 77 Hz and 1 kHz, as shown in Figure 6.9 (c). The sensor exhibits two distinct linear trends at both frequencies. At 77 Hz, the sensor response increases smoothly as the antigen concentration rises from 3.92 ng mL^{-1} to 88.43

ng mL^{-1}. Beyond this point, the steady capacitance response from 88.43 ng mL^{-1} to 445.76 ng mL^{-1}, ultimately reaching a saturation point where additional antigen does not significantly alter the capacitance. Similarly, at 1 kHz, the sensor response increases rapidly within the range of 3.92 ng mL^{-1} to 86.08 ng mL^{-1} before stabilizing between 86.08 ng mL^{-1} and 445.76 ng mL^{-1} and eventually saturating at higher concentrations. This behaviour indicates that the sensor is highly responsive to antigen concentrations within these ranges and demonstrates excellent linearity and sensitivity before saturation occurs. The relationship between the antigen concentration and the change in capacitance can be demonstrated using the adsorption isotherm equation 5.2, displayed in chapter 5, where the terms have their usual meaning. To further analyze the sensor's performance, the inverse of capacitance **(**$1/\Delta C_p$**)** is plotted against the inverse of antigen concentration **(**$1/\Delta$Conc.**)** for both frequencies (Figure 6.9 (d)). The linear regression from these plots allows for the determination of the LOD of the sensor [30].

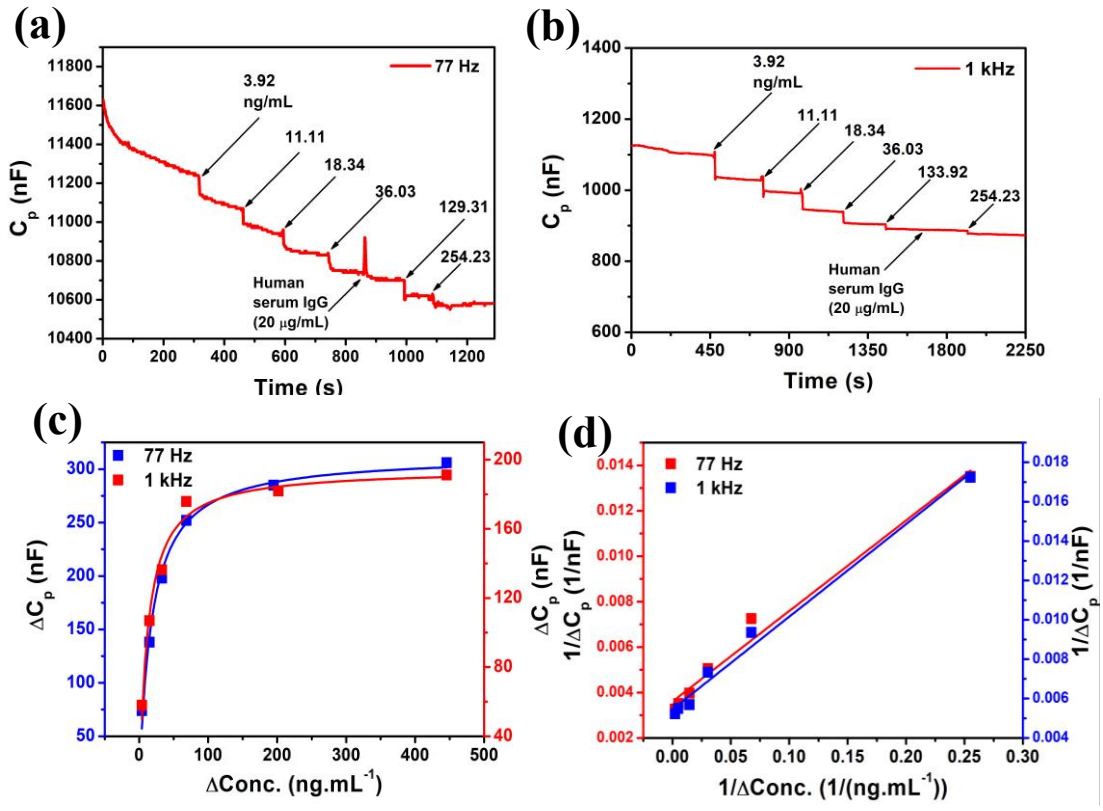

Figure 6.9: Transient capacitance plot of anti-AF-B_1/GLU/PANI-PVA based AF-B_1 sensors at (a) 77 Hz (b) 1 kHz. (c) Adsorption plot and (d) Linear regression plot of PANI-PVA capacitive sensor at 77 Hz and 1 kHz.

The calculated LODs are 12.82 ng mL^{-1} (equivalent to 85 pM) at 77 Hz and 18.57 ng mL^{-1} (equivalent to 123 pM) at 1 kHz. These values highlight the ability of the sensor to detect low concentrations of AF-B_1 with high precision. Furthermore, the response of the sensor, which is defined as the change in capacitance per unit of antigen concentration, was estimated to be 25.64 $nFng^{-1}mL$ at 77 Hz and 21.27 $nFng^{-1}mL$ at 1 kHz. This result indicates that the sensor is more sensitive at lower frequencies, as evidenced by the higher response value at 77 Hz. The higher sensitivity at 77 Hz makes it the ideal frequency for detecting noticeable changes in capacitance due to antigen-antibody interactions, especially in a label-free immunosensor where signal amplification through enzymes or redox agents is not used.

Therefore, the proposed immunosensor demonstrates excellent sensitivity, selectivity, and linear response across a wide concentration range, making it highly effective for detecting AF-B_1. The use of transient capacitance measurements at two frequencies allows for a comprehensive analysis of the sensor's behaviour, with 77 Hz offering superior sensitivity.

6.9. Repeatability

For the development of a reliable biosensor, repeatability studies were conducted using different PANI-PVA-based electrodes at two distinct frequencies: 77 Hz and 1 kHz. To ensure the reliability of the results, the experiments were performed under identical optimized conditions using three separate electrodes. This approach allowed for a comprehensive evaluation on the consistency performance of the sensor. The repeatability of the biosensor was confirmed by analyzing the data obtained from these experiments, with the findings demonstrating strong repeatability, as indicated in Table 6.4. The LOD was determined to be approximately~13 ng mL^{-1} at 77 Hz and~19 ng mL^{-1} at 1 kHz.

Additionally, the linear relationship between the inverse of the change in capacitance ($1/\Delta C_p$) and the inverse of the change in concentration ($1/\Delta$Conc.) was plotted for both frequencies, with error bars representing the variability in the measurements. The resulting linear plots, as shown in Figure 6.10, further support the repeatability and robustness of the sensor. The error bars provide visual confirmation that the measurements across different electrodes remain within an acceptable range of variability, reinforcing the reliability of the performance of the sensor at both 77 Hz and 1 kHz.

Table 6.4: Results from repeated experiments for AF-B_1 capacitive sensor (both at 77 Hz and 1 kHz).

Serial number	Electrode	Frequency, Hz	LOD, (ng mL^{-1})	Sensitivity, ($nFng^{-1}mL$)	Linear range, (ng mL^{-1})
1	PANI-PVA, sensor 1	77	12.82	25.64	3.92-445.76
2	PANI-PVA, sensor 2	77	13.21	21.58	3.92-445.76
3	PANI-PVA, sensor 3	77	12.95	23.66	3.92-445.76
4	PANI-PVA, sensor 1	1000	18.57	21.27	3.92-445.76
5	PANI-PVA, sensor 2	1000	19.82	21.66	3.92-445.76
6	PANI-PVA, sensor 3	1000	18.98	20.78	3.92-445.76

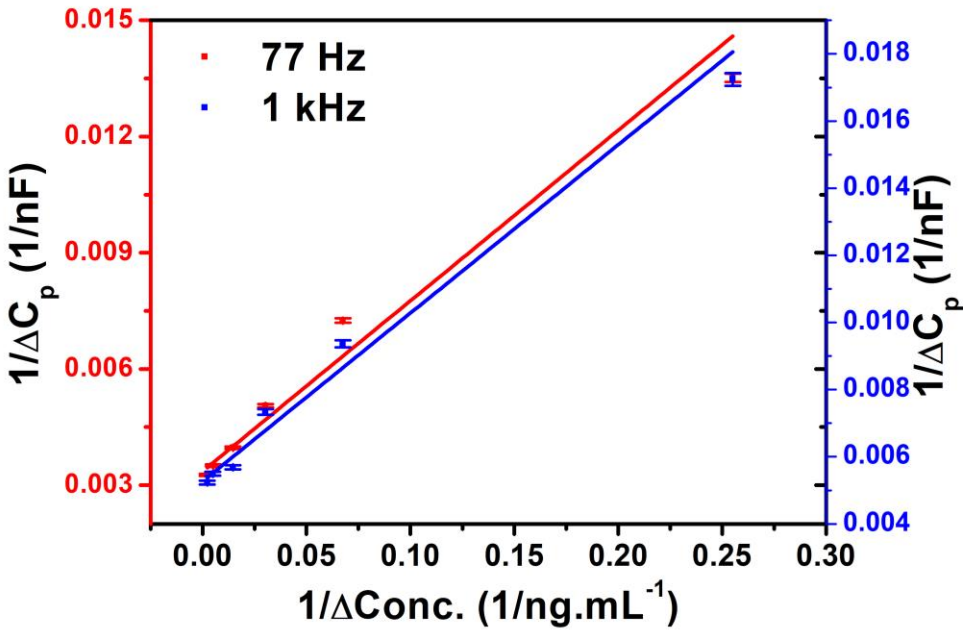

Figure 6.10: Linear regression plot of PANI-PVA capacitive sensors at 77 Hz and 1 kHz; with error bar.

6.10. Detection of AF-B_1 via Differential Pulse Voltammetry

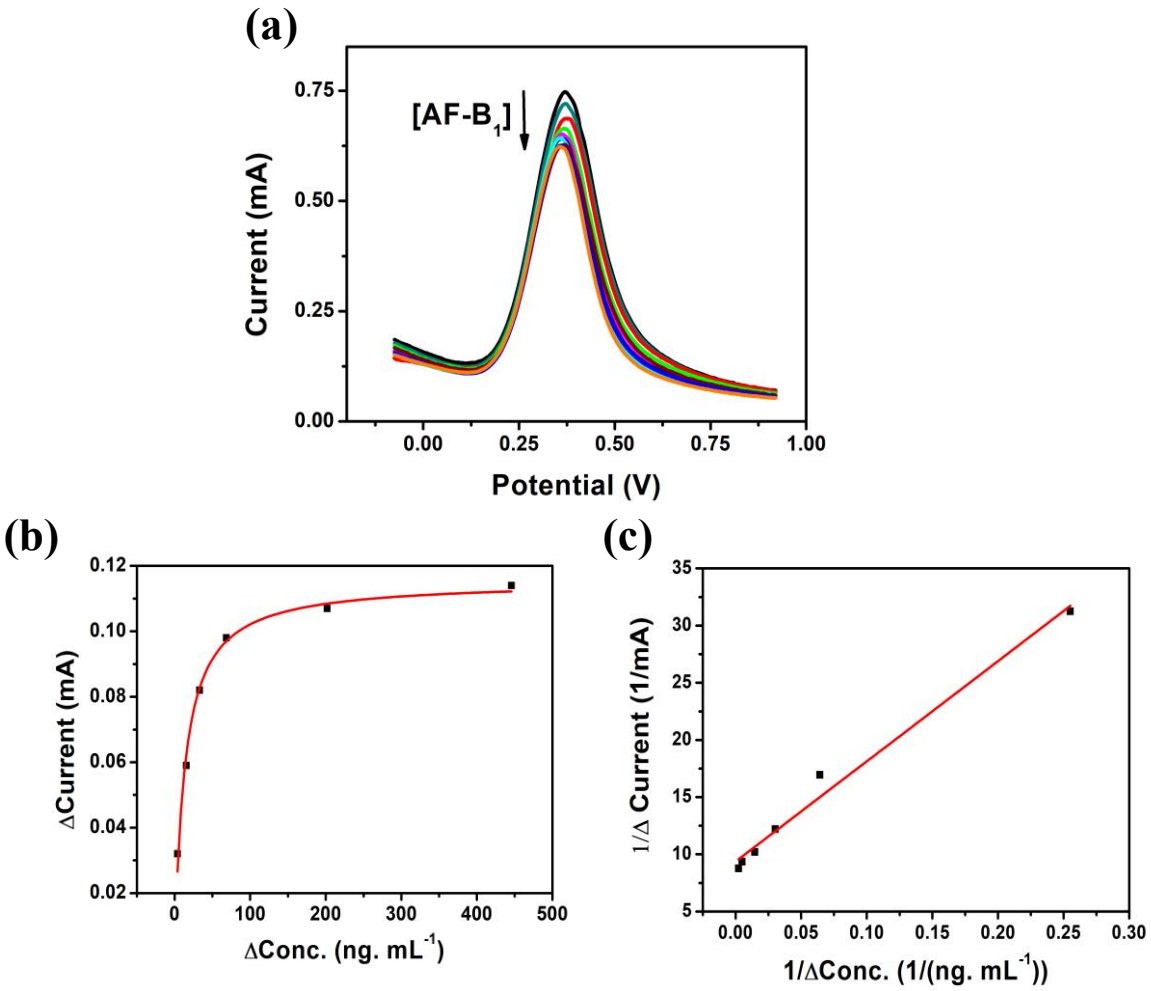

Figure 6.11: DPV plot of BSA/anti-AF-B_1/GLU/PANI-PVA/ITO with different concentration of AF-B_1 (3.92 ng mL^{-1}-690 ng mL^{-1}) (b) Adsorption isotherm plot. (c) Linear regression plot for 1/ΔConc. vs. 1/ΔCurrent.

Another detection technique, DPV, was conducted to evaluate the performance of the immunosensor for detecting AF-B_1, using an anti-AF-B_1 immobilized GLU/PANI-PVA/ITO bioelectrode. To be mentioned, DPV is an advanced electrochemical technique that allows for the investigation of amperometric responses, making it particularly suitable for studying the interactions between the sensor and target analytes. The DPV measurements were performed in a three-electrode setup, where the potential was swept from -0.2 V to 0.8 V, utilizing a solution of 500 mM $[Fe(CN)_6]^{3-/4-}$ combined with 100 mM PBS as an electrolyte. In this study, the DPV responses of PANI-PVA electrode modified with antibody anti-AF-B_1 was examined across varying concentrations of AF-

B_1, as illustrated in Figure 6.11 (a). The DPV plot revealed a systematic decrease in the current response as the concentration of AF-B_1 increased, indicating a specific interaction between the immobilized anti-AF-B_1 antibodies and the target AF-B_1 molecules. This interaction leads to the formation of antibody-antigen complexes on the bioelectrode, which hinders the electron transfer between the redox probe $[Fe(CN)_6]^{3-/4-}$ and the electrode surface. Subsequently, the change in the DPV peak current for the BSA/anti-AF-B_1/GLU/PANI-PVA/ITO electrode was plotted against the corresponding changes in AF-B_1 concentration, as shown in Figure 6.11 (b). The relationship between the change in current and change in concentration was analyzed using the Langmuir adsorption isotherm as discussed in chapter 5. The results depicted in Figure 6.11 (b) demonstrate a linear and rapid response at lower AF-B_1 concentrations, ranging from 3.92 ng mL^{-1} to 99.86 ng mL^{-1}. As the concentration increased beyond this point, the response reached a steady state between 99.87 ng mL^{-1} and 445.76 ng mL^{-1}, ultimately saturating with no further increase in current response. A linear regression analysis between the inverse of Δ Current and the inverse of Δ Conc., shown in Figure 6.11 (c), yielded a high correlation coefficient (R^2 = 0.9827), confirming the reliability of the data.

The detection limit of the sensor was found as 17.85 ng mL^{-1} (119 pM) [30]. Additionally, the estimated sensitivity of the proposed sensor was calculated to be 11.49 $\mu Ang^{-1}mL$, further highlighting its effectiveness for AF-B_1 detection in practical applications. Overall, these findings illustrate the immunosensor's potential for precise and sensitive detection of AF-B_1, making it a valuable tool for monitoring this harmful toxin in various samples.

6.11. Reliability and selectivity test

The results, as outlined in Table 6.5, demonstrate consistent and comparable performance across repeated experiments using different PANI-PVA/ITO electrodes. This repeatability indicates the robustness of the experimental procedure, where minimal variation is observed between different trials. For the BSA/anti-AF-B_1/GLU/PANI-PVA/ITO electrode, the data presented in Figure 6.12, which includes a linear plot with error bars, further validates the accuracy and precision of the sensor response. The error bars show the standard deviation, indicating a small variation between measurements and confirming that the experimental setup produces consistent results. The LOD, found to be within the range of 9-12 ng mL^{-1} (60-80 pM), highlights the sensitivity of the sensor in detecting low

concentrations of the target analyte. This range aligns well with the expected sensitivity for such bio-sensing platforms, designed to detect trace levels of substances (upto ppm, ppb), which is crucial for applications in fields like diagnostics and environmental monitoring.

Table 6.5: Repeated experiments result for PANI-PVA based AF-B_1 sensor using amperometry technique, DPV.

Serial number	Electrode	LOD, (ng mL^{-1})	Sensitivity, (μAng^{-1} mL)	Linear range, (ng mL^{-1})
1	PANI-PVA, sensor 1	17.85	11.49	3.92-445.76
2	PANI-PVA, sensor 2	17.92	10.35	3.92-445.76
3	PANI-PVA, sensor 3	18.68	9.98	3.92-445.76

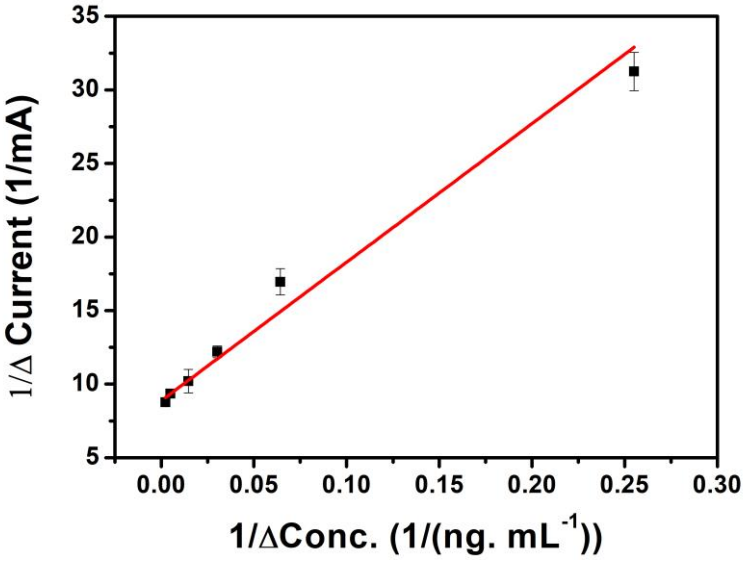

Figure 6.12: 1/ΔI vs. 1/ΔConc. for the BSA/anit-AF-B_1/GLU/PANI-PVA sensor along with linear regression plot with error bar w.r.to standard deviation.

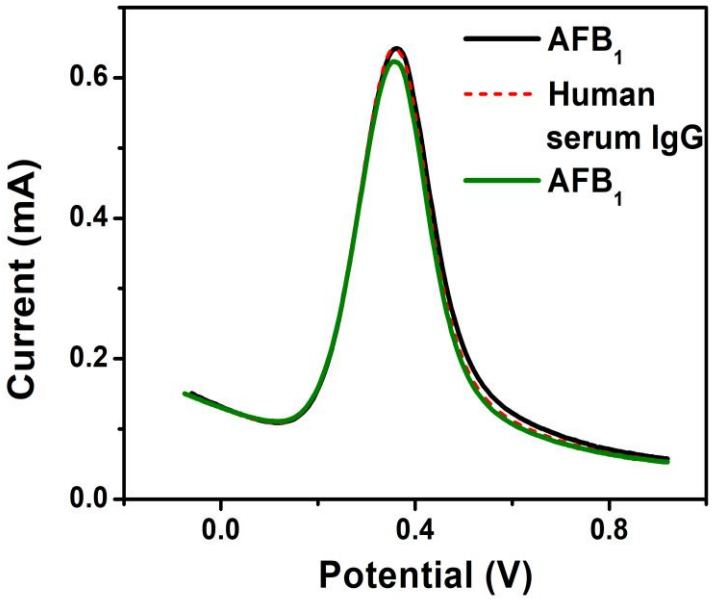

Figure 6.13: Selectivity test of BSA/anit-AF-B_1/GLU/PANI-PVA sensor.

Moreover, the comparison between the capacitive and DPV methods shows that both techniques provide similar results, reinforcing the reliability of the developed sensor. The agreement between these methods emphasizes the versatility of the sensor and its applicability across different measurement techniques. The consistency across multiple platforms strengthens assurance in the performance of the sensor, further highlighting its potential for practical applications.

The selectivity of the sensor was assessed by introducing human serum IgG, a non-specific protein, to evaluate its response to potential interfering substances. When human serum IgG was injected, there was no noticeable change or shift in the DPV peak current, as demonstrated in Figure 6.13. This lack of response indicates that the sensor does not interact with or detect non-target molecules, confirming its high selectivity. As a result, the sensor is shown to be highly specific to its target analyte, AF-B_1, ensuring that it can effectively distinguish AF-B_1 even in the presence of other proteins or interfering agents. This selectivity is crucial for reliable detection in complex biological samples, where non-specific interactions could otherwise lead to inaccurate measurements.

6.12. Real sample test

To validate the performance of the BSA/anti-AF-B_1/GLU/PANI-PVA/ITO immunosensor, DPV measurements were conducted on real samples. The samples tested included white button mushrooms (*Agaricus bisporus*), and okra (*Abelmoschus esculentus*). The

preparation of these real samples (both mushrooms and okra) for testing is presented in Chapter 4. The DPV was performed on PBS solutions used to wash freshly harvested mushrooms as well as mushrooms that had been exposed to air for one, two, and three days with increasing volumes 50, 100, 200, and 300 µL. The DPV current responses corresponding to the mushrooms exposed to air for different days with incremental spiking (50-300 µL) is displayed in Figures 6.14 (a-d). The change in DPV peak current as a function of the number of days the mushrooms were exposed to air is depicted in Figure 6.15.

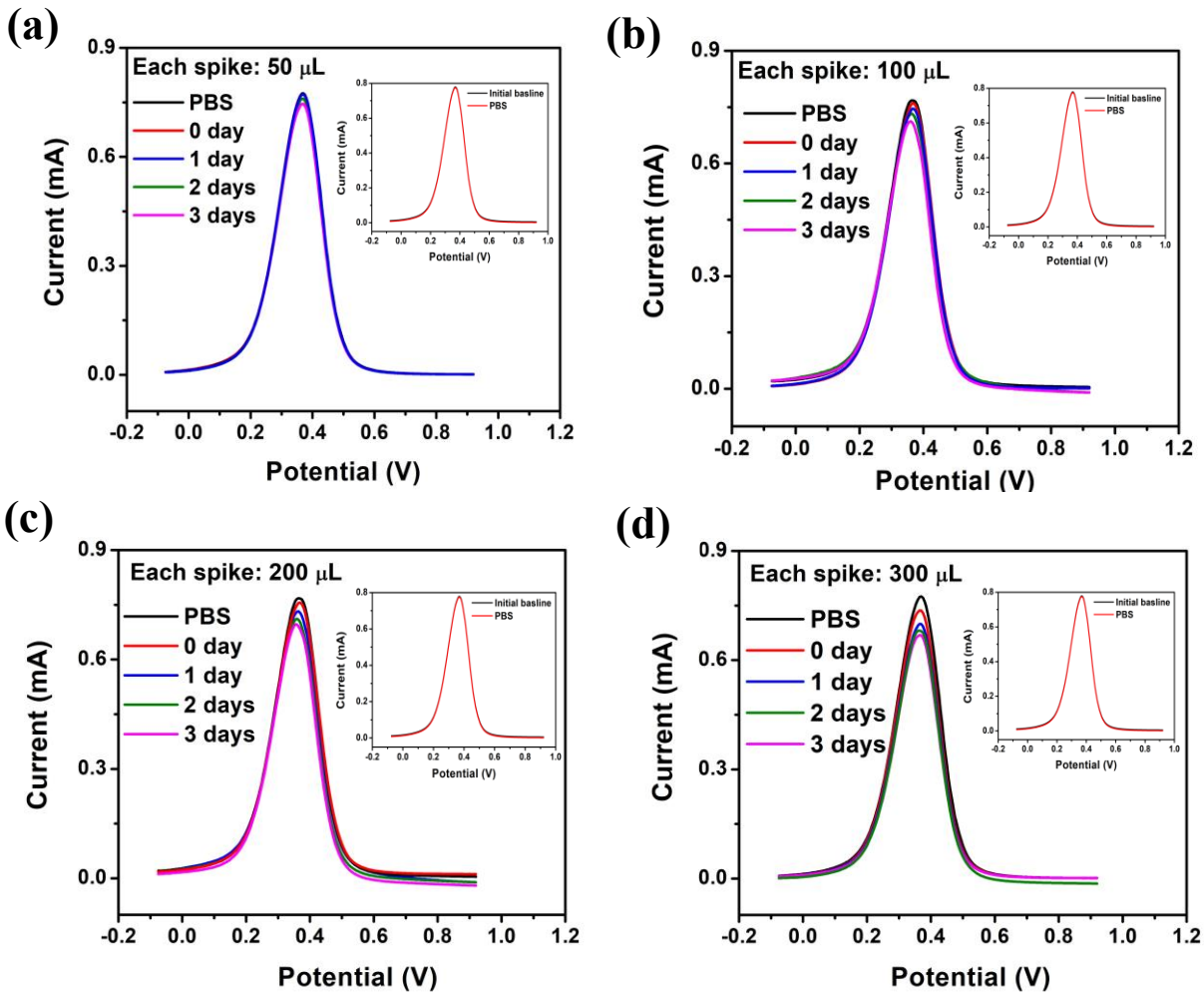

Figure 6.14: DPV pattern of PANI-PVA/ITO composite electrode towards mushrooms (kept exposed to air 20 ºC for 0-3 days and washed with PBS) with different spiking volumes (50-200) µL, (a) 50 µL (b) 100 µL, (c) 200 µL (d) 300 µL. Inset shows the voltammogram after addition of 200 µL PBS.

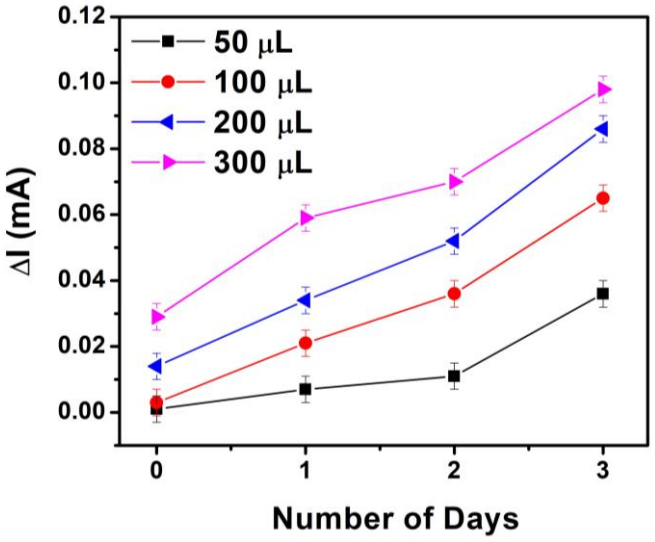

Figure 6.15: Change in peak current vs number of days of air exposure for mushrooms.

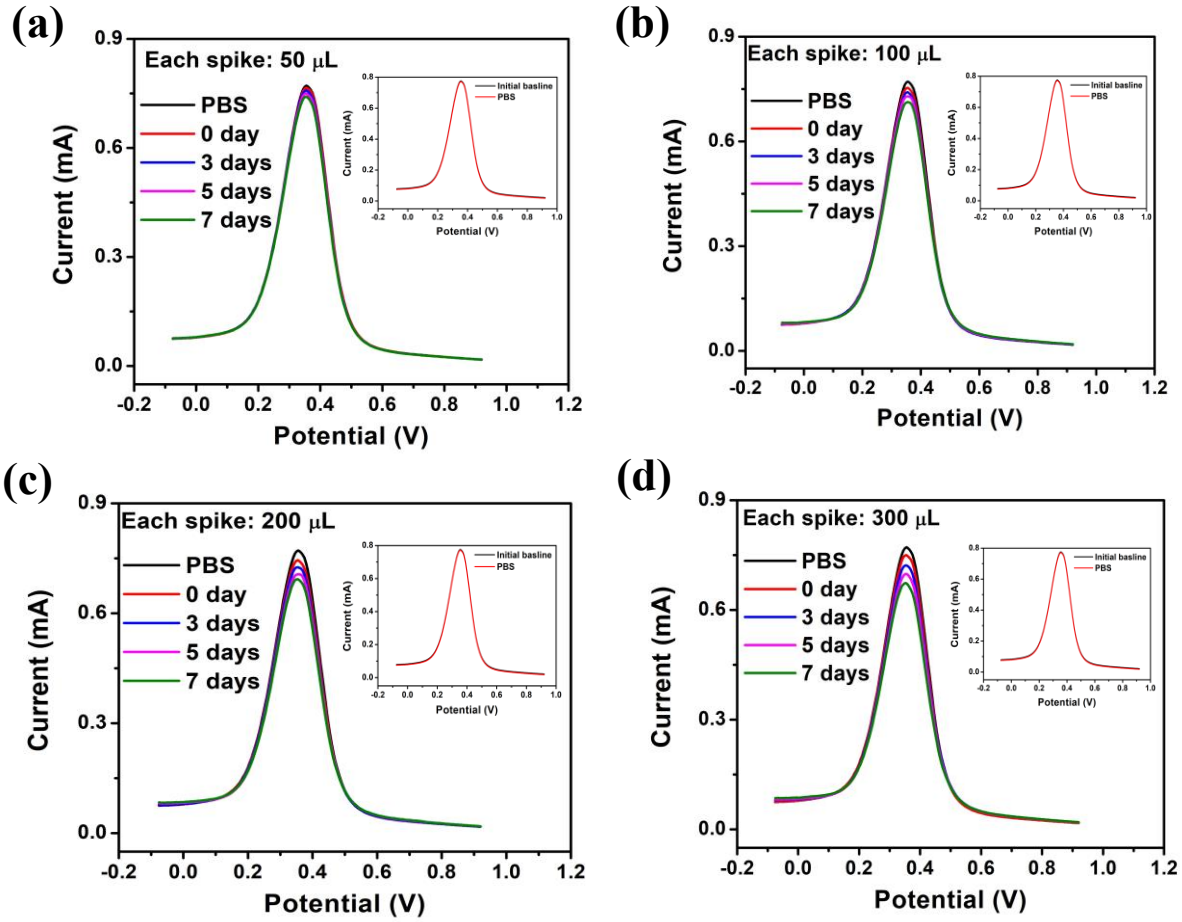

Figure 6.16: DPV pattern of PANI-PVA/ITO composite electrode towards okra (kept exposed to air 24 ºC for 0-7 days and washed with PBS) with different spiking volumes (50-200) µL, (a) 50 µL (b) 100 µL, (c) 200 µL, (d) 300 µL. Inset of each figure shows the voltammogram after addition of 200 µL PBS.

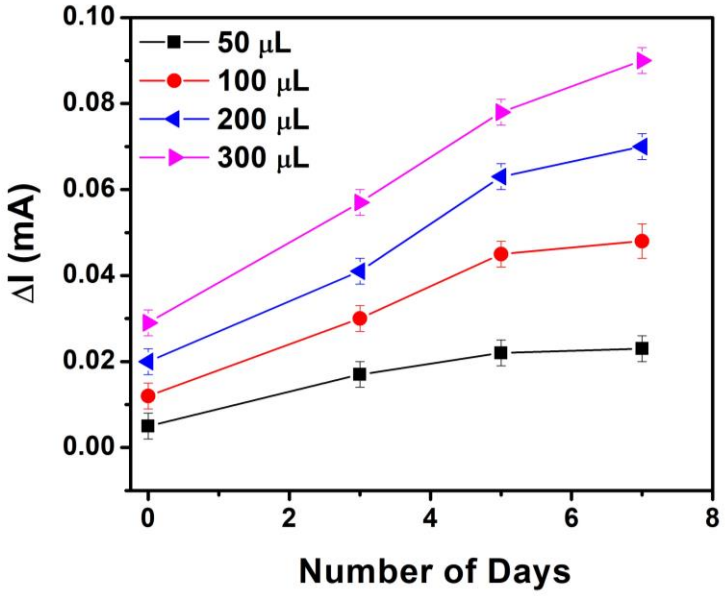

Figure 6.17: Change in peak current vs number of days of air exposure for okra.

The Figure demonstrates the increase in AF-B_1 concentration, with the peak current indicating the presence of 72.01 ng mL^{-1} of AF-B_1 in mushrooms after three days of air exposure at room temperature (Figure 6.15).

Similarly, DPV measurements were carried out using PBS solutions employed to wash fresh okra and okra that had been exposed to air for three, five, and seven days. Incremental spiking of AF-B_1 (50, 100, 200, and 300 µL) was performed, and the corresponding DPV current responses were recorded, shown in Figures 6.16 (a-d). The relationship between DPV peak current and the number of days of air exposure okra is shown in Figure 6.17, which indicates the presence of 56.67 ng mL^{-1} of AF-B_1 in okra after seven days of air exposure at room temperature.

The immunosensor exhibited a clear and consistent DPV current response to the incremental spiking of AF-B_1 in both mushroom and okra samples. The decrease in DPV peak current with spiking and air exposure days suggests that the immunosensor effectively detects the presence of AF-B_1 without interference from other compounds in the real samples. This demonstrates the immunosensor's ability to reliably monitor AF-B_1 levels in perishable foods over time, highlighting its scope for practical applications in food safety monitoring. The sensor showed no significant obstructions or interference in detection of AF-B_1 contamination in food samples during DPV measurements, indicating its potential for real-time, on-site monitoring.

6.13. Conclusions

The development of nanofiber-based PANI-PVA/ITO electrodes has proven to be a highly sensitive, selective, and reliable platform for biosensing applications, specifically for much needed glucose and AF-B_1 detection. The unique properties of the PANI-PVA nanofiber matrix, such as its excellent electroactive behavior, large surface area, and efficient charge transfer capabilities, have greatly enhanced the sensing performance of these electrodes. In glucose sensing, the *GlOx*/GLU/PANI-PVA/ITO biosensor demonstrated rapid and consistent response characteristics with remarkable linearity over a broad range of glucose concentrations (0.19 to 455.42 µM). The LOD was estimated as low as 1.65 µM, and its sensitivity was calculated to be 11.7 µA μM^{-1}. The biosensor also exhibited exceptional selectivity toward glucose, making it a suitable candidate for practical applications, as demonstrated by its fruitful testing in human saliva samples. The incorporation of glutaraldehyde as a crosslinker in the functionalization process further stabilized the immobilization of the glucose oxidase enzyme, ensuring a robust and consistent sensing mechanism. For AF-B_1 detection, the label-free immunosensor fabricated by immobilizing anti-AF-B_1 onto the PANI-PVA/ITO platform, in the presence of a glutaraldehyde crosslinker, showed excellent electrochemical properties. Electrochemical characterization via CV and EIS revealed superior charge transfer kinetics and electroactive behavior, essential for reliable detection. Two sensing techniques, transient capacitance and DPV, were employed to evaluate the sensor's performance, with highly comparable results. Transient capacitance measurements yielded responses of 25.64 $nFng^{-1}$ mL at 77 Hz and 21.27 $nFng^{-1}mL$ at 1 kHz, demonstrating high sensitivity with corresponding LODs of 12.82 ng mL^{-1} (85 pM) and 18.57 ng mL^{-1} (123 pM), respectively. The concentration range extended from 3.92 ng mL^{-1} to 445.76 ng mL^{-1} at both 77 Hz and 1 kHz, making this sensor highly effective for detecting a wide range of AF-B_1 concentrations. Amperometric sensing using DPV provided notable results, with similar concentration range of 3.92 ng mL^{-1} to 445.76 ng mL^{-1} and a sensitivity of 11.49 $\mu Ang^{-1}mL^{-1}$. The LOD for AF-B_1 detection via DPV was calculated to be 17.85 ng mL^{-1} (119 pM), confirming the immunosensor's ability to detect AF-B_1 at extremely low concentration. The selectivity of the sensor was also thoroughly examined by testing against non-specific human serum IgG, and the immunosensor demonstrated excellent selectivity toward AF-B_1. The comparison of sensing parameters between the capacitive

and amperometric methods showed remarkable consistency, augmenting the reliability and accuracy of the sensor across different detection techniques. Real sample analysis using mushroom and okra further validated the practical application of this sensor, providing an effective solution for the on-site detection of AF-B_1, a major food contaminant. The tremendous performance of these biosensors can be attributed to the properties of the PANI-PVA nanofibers. The nanofibrous structure offers a significantly increased surface area, which enhances the immobilization of biomolecules such as enzymes (*GlOx*) and antibodies (anti-AF-B_1). The high porosity of the nanofibers allows better diffusion of analytes, ensuring rapid and efficient interaction between the target molecules and the sensor surface. Additionally, the nanofiber matrix facilitates superior charge transfer, improving the sensitivity and detection limits of the biosensors. The remarkable flexibility, mechanical stability, and electrochemical properties of the PANI-PVA nanofibers make them an excellent choice for fabricating advanced biosensors. The use of nanofiber technology with advanced electrochemical methods has led to the development of a highly versatile and technologically efficient biosensing platform. These sensors hold great promise for real-world applications, particularly in health monitoring and food safety control, offering a powerful tool for sensitive, on-site detection of glucose and harmful contaminants like AF-B_1.

6.14. References

[1] Wang, P., Du, M., Zhang, M., Zhu, H., Bao, S., Zou, M., and Yang, T. Facile fabrication of AuNPs/PANI/HNTs nanostructures for high-performance electrochemical sensors towards hydrogen peroxide. *Chemical Engineering Journal*, 248:307-314, 2014.

[2] Abd Razak, S. I., Wahab, I. F., Fadil, F., Dahli, F. N., Md Khudzari, A. Z., and Adeli, H. A review of electrospun conductive polyaniline based nanofiber composites and blends: processing features, applications, and future directions. *Advances in Materials Science and Engineering*, 2015(1):356286, 2015.

[3] Kaewda, C., and Sriwichai, S. Label-Free Electrochemical Dopamine Biosensor Based on Electrospun Nanofibers of Polyaniline/Carbon Nanotube Composites. *Biosensors*, 14(7):349, 2024.

[4] Santhosh, P., Manesh, K. M., Lee, S. H., Uthayakumar, S., Gopalan, A. I., and Lee, K. P. Sensitive electrochemical detection of superoxide anion using gold nanoparticles distributed poly (methyl methacrylate)–polyaniline core–shell electrospun composite electrode. *Analyst*, 136(8):1557-1561, 2011.

[5] Andre, R. S., Pavinatto, A., Mercante, L. A., Paris, E. C., Mattoso, L. H., and Correa, D. S. Improving the electrochemical properties of polyamide 6/polyaniline electrospun nanofibers by surface modification with ZnO nanoparticles. *RSC advances*, 5(90):73875-73881, 2015.

[6] Mercante, L. A., Iwaki, L. E., Scagion, V. P., Oliveira Jr, O. N., Mattoso, L. H., and Correa, D. S. Electrochemical detection of bisphenol a by tyrosinase immobilized on electrospun nanofibers decorated with gold nanoparticles. *Electrochem*, 2(1):41-49, 2021.

[7] Kailasa, S., Reddy, M. S. B., Maurya, M. R., Rani, B. G., Rao, K. V., and Sadasivuni, K. K. Electrospun nanofibers: materials, synthesis parameters, and their role in sensing applications. *Macromolecular Materials and Engineering*, 306(11):2100410, 2021.

[8] Ramya, R. and Sangaranarayanan, M. V. Electrochemical sensing of glucose using polyaniline nanofiber dendrites-amperometric and impedimetric analysis. *Journal of applied polymer science*, 129(2):735-747, 2013.

[9] Castagna, R., Tunesi, M., Saglio, B., Della Pina, C., Sironi, A., Albani, D., ... and Falletta, E. Ultrathin electrospun PANI nanofibers for neuronal tissue engineering. *Journal of Applied Polymer Science*, 133(35):43885, 2016.

[10] Shoaie, N., Daneshpour, M., Azimzadeh, M., Mahshid, S., Khoshfetrat, S. M., Jahanpeyma, F., ... and Foruzandeh, M. Electrochemical sensors and biosensors based on the use of polyaniline and its nanocomposites: A review on recent advances. *Microchimica Acta*, *186*(7):465, 2019.

[11] Malara, A., Fotia, A., Paone, E., and Serrano, G. Electrospun nanofibers and electrochemical techniques for the detection of heavy metal ions. *Materials*, 14(11):3000, 2021.

[12] Migliorini, F. L., Sanfelice, R. C., Mercante, L. A., Facure, M. H., and Correa, D. S. Electrochemical sensor based on polyamide 6/polypyrrole electrospun nanofibers coated with reduced graphene oxide for malathion pesticide detection. *Materials Research Express*, 7(1):015601, 2020.

[13] Halicka, K., and Cabaj, J. Electrospun nanofibers for sensing and biosensing applications—A review. *International Journal of Molecular Sciences*, 22(12):6357, 2021.

[14] Wang, J., and Zhang, D. One-Dimensional Nanostructured Polyaniline: Syntheses, Morphology Controlling, Formation Mechanisms, New Features, and Applications. *Advances in Polymer Technology*, 32(S1):E323-E368, 2013.

[15] Bavatharani, C., Muthusankar, E., Wabaidur, S. M., Alothman, Z. A., Alsheetan, K. M., mana AL-Anazy, M., and Ragupathy, D. Electrospinning technique for production of polyaniline nanocomposites/nanofibres for multi-functional applications: A review. *Synthetic Metals*, 271:116609, 2021.

[16] Chang, G., Luo, Y., Lu, W., Qin, X., Asiri, A. M., Al-Youbi, A. O., and Sun, X. Ag nanoparticles decorated polyaniline nanofibers: synthesis, characterization, and applications toward catalytic reduction of 4-nitrophenol and electrochemical detection of H_2O_2 and glucose. *Catalysis Science & Technology*, 2(4):800-806, 2012.

[17] Wang, Y. Preparation and application of polyaniline nanofibers: an overview. *Polymer International*, 67(6):650-669. 2018.

[18] Shoaie, N., Daneshpour, M., Azimzadeh, M., Mahshid, S., Khoshfetrat, S. M., Jahanpeyma, F., ... and Foruzandeh, M. Electrochemical sensors and biosensors based on the use of polyaniline and its nanocomposites: A review on recent advances. *Microchimica Acta*, 186:1-29, 2019.

[19] Lee, J. H., and Hong, H. G. Nonenzymatic electrochemical sensing of hydrogen peroxide based on a polyaniline-MnO2 nanofiber-modified glassy carbon electrode. *Journal of Applied Electrochemistry*, 45:1153-1162, 2015.

[20] Hou, X., Zhou, Y., Liu, Y., Wang, L., and Wang, J. Coaxial electrospun flexible PANI//PU fibers as highly sensitive pH wearable sensor. *Journal of Materials Science*, *55*:16033-16047, 2020.

[21] Chokkiah, B., Eswaran, M., Wabaidur, S. M., Alothman, Z. A., Lee, S. C., and Dhanusuraman, R. An efficient amperometric sensor for chloride ion detection through electroactive e-spun PVA-PANi-g-C3N4 nanofiber. *Journal of Materials Science: Materials in Electronics*, 33(12):9425-9437, 2022.

[22] Asmatulu, R., Veisi, Z., Uddin, M. N., and Mahapatro, A. Highly sensitive and reliable electrospun polyaniline nanofiber based biosensor as a robust platform for COX-2 enzyme detections. *Fibers and Polymers*, 20:966-974, 2019.

[23] Kang, S., Zhao, K., Yu, D. G., Zheng, X., and Huang, C. Advances in biosensing and environmental monitoring based on electrospun nanofibers. *Advanced Fiber Materials*, 4(3):404-435, 2022.

[24] Fenniche, F., Khane, Y., Henni, A., Aouf, D., and Djafri, D. E. Synthesis and characterization of PANI nanofibers high-performance thin films via electrochemical methods. *Results in Chemistry*, 4:100596, 2022.

[25] Betty, C. A. Highly sensitive capacitive immunosensor based on porous silicon–polyaniline structure: Bias dependence on specificity. *Biosensors and Bioelectronics*, 25(2):338-343, 2009.

[26] German, N., Ramanaviciene, A., and Ramanavicius, A. Formation and electrochemical evaluation of polyaniline and polypyrrole nanocomposites based on glucose oxidase and gold nanostructures. *Polymers*, 12(12):3026, 2020.

[27] Jose, M. V., Marx, S., Murata, H., Koepsel, R. R., and Russell, A. J. Direct electron transfer in a mediator-free glucose oxidase-based carbon nanotube-coated biosensor. *Carbon*, 50(11):4010-4020, 2012.

[28] Christwardana, M., Chung, Y., and Kwon, Y. A correlation of results measured by cyclic voltammogram and impedance spectroscopy in glucose oxidase based biocatalysts. *Korean Journal of Chemical Engineering*, 34:3009-3016, 2017.

[29] Zhang, X., Liu, D., Li, L., and You, T. Direct electrochemistry of glucose oxidase on novel free-standing nitrogen-doped carbon nanospheres@ carbon nanofibers composite film. *Scientific reports*, 5(1):9885, 2015.

[30] Shrivastava, A., and Gupta, V. B. Methods for the determination of limit of detection and limit of quantitation of the analytical methods. *Chronicles of Young Scientists*, 2(1):21-25, 2011.

[31] Sharma, A., Kumar, A., and Khan, R. A highly sensitive amperometric immunosensor probe based on gold nanoparticle functionalized poly (3, 4-ethylenedioxythiophene) doped with graphene oxide for efficient detection of aflatoxin B_1. *Synthetic Metals*, 235:136-144, 2018.